The influence of surface fluorination in the photocatalytic behaviour of TiO$_2$ aqueous dispersions: An analysis in the light of the direct–indirect kinetic model

J.F. Montoya [a], P. Salvador [b,c,*]

[a] Departamento de Química, Universidad Autónoma de Barcelona, Spain
[b] Departament de Ciències Matemàtiques i Informàtica, Universitat de les Illes Balears, Palma de Mallorca, E-07071, Spain
[c] Instituto de Católisis y Petroleoquímica, CSIC, Spain

ABSTRACT

TiO$_2$ surface fluorination is known to produce an enhancement of the photocatalytic oxidation rate of some organic compounds such as phenol, acid orange, azo dye Acid Red 1 and benzoic acid, while leads to a clear decrease of the photooxidation quantum yield of other compounds like formic acid, and dichloroacetate. Here we show that these differences in behaviour cannot be explained in the framework of the classical "Langmuir–Hinshelwood" (L–H) kinetic model, although they are compatible with the predictions of the alternative, recently developed "Direct–Indirect"(D–I) model [19]. For weak electronic interaction of the TiO$_2$ surface with dissolved substrate species, as it is for instance the case for phenol, the D–I model predicts that photooxidation takes place mainly via an interfacial, indirect transfer (IT) mechanism involving inelastic trapping of valence band free holes by terminal, twofold coordinated oxygen ions, and further adiabatic transfer to dissolved substrate species. On the basis of open-circuit voltage measurements, the origin of the photooxidation quantum yield increase observed in these cases when the TiO$_2$ surface becomes fluorinated is attributed to the partial substitution of water molecules adsorbed on terminal Ti sites by fluoride ions, leading to: (1) an interfacial decrease of the electron-hole recombination rate as the surface concentration of recombination centres associated with terminal Ti sites diminishes; (2) an increase of the IT rate of surface trapped holes to reduced dissolved species, because of the upward shift experimented by the semiconductor energy levels with respect to filled electrolyte energy levels. In contrast, for strong electronic interaction of substrate species with the naked TiO$_2$ surface, as it is for instance the case of formate ions at low enough pH, photooxidation mainly take place via an interfacial, direct transfer (DT) mechanism, involving inelastic trapping of valence band free holes by specifically adsorbed substrate species. The photooxidation quantum yield decrease observed in this case is explained to be due to a diminution of the density of TiO$_2$ surface sites active for adsorption of formate ions. The enhanced photogeneration of free OH$_S^\bullet$ radicals and/or photooxidation rate of water molecules in the liquid phase with free VB holes, assumed by some authors as the origin of the observed photooxidation quantum yield increase at the fluorinated TiO$_2$ surface, should be disregarded as far as both processes appears to be thermodynamically and kinetically hindered.

© 2009 Elsevier B.V. All rights reserved.

1. Introduction

The photocatalytic properties of semiconductors are greatly influenced by their surface composition and structure, as far as the efficiency of photoinduced charge transfer process taking place at the semiconductor-aqueous electrolyte interface is affected [1]. For instance, the presence of dissolved inorganic anions is known to affect the mineralization processes of organic compounds under photocatalytic conditions [2]. In particular, surface fluorination (i.e., specific adsorption of fluoride ions on terminal Ti atoms), which is different than F$^-$ doping (i.e., substitution of F$^-$ for O^{2-} lattice ions), strongly modifies the TiO$_2$ surface properties. The specific adsorption of fluoride anions on the semiconductor surface at acidic pH leads to the formation of Ti$_S$–F$^{1/3-}$ surface states with displacement of water molecules single bonded to terminal Ti cations, according to the surface exchange reaction (1) [3], written according to the Multisite Complexation (MUSIC) model introduced by Hiemstra et al. [4,5]

$$Ti_S - OH_2^{2/3+} + F_{aq}^- \Leftrightarrow Ti_S - F^{1/3-} + H_2O \tag{1}$$
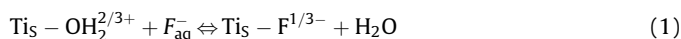
where super index indicates formal charge of ions specifically adsorbed on terminal Ti atoms.

* Corresponding author at: Departament de Ciències Matemàtiques i Informàtica, Universitat de les Illes Balears, Palma de Mallorca, E-07071, Spain.
E-mail address: dmipss9@uib.es (P. Salvador).

Nomenclature

ϕ	incident photon flux ($cm^{-2}\,s^{-1}$)
V_{fb}	semiconductor flat band potential (V)
C_{sc}	layer capacitance (F)
$[F_S^-]$	surface concentration of adsorbed fluoride ions (cm^{-2})
E_{st}^*	steady-state open-circuit potential under illumination (V)
$[e_f^-]$	concentration of conduction band free electrons (cm^{-3})
$[h_f^+]$	concentration of valence band free holes (cm^{-3})
$[h_S^+]$	concentration of surface trapped holes (cm^{-3})
$[Ti_S^{III}]$	concentration of Titanium surface states with oxidation degree III (cm^{-3})
$[Ti_S^{IV}]$	concentration of Titanium surface states with oxidation degree IV (cm^{-3})
$[RH_2]_{aq}$	aqueous concentration of organic species (cm^{-3})
$[RH_2]_S$	TiO$_2$ surface density of chemisorbed organic species (cm^{-2})
$[PhO]_{aq}$	aqueous concentration of phenol species (cm^{-3})
$[PhO]_S$	TiO$_2$ surface density of chemisorbed phenol species (cm^{-2})
$[FA]_{aq}$	aqueous concentration of formic acid species (cm^{-3})
$[O_S^{2-}]$	TiO$_2$ surface density of terminal oxygen ions (cm^{-2})
A	Langmuir adsorption constant (cm^3)
B	density of surface sites available for adsorption of dissolved substrate species (cm^{-2})
V_0	photogeneration rate of free electron-hole pairs ($cm^{-3}\,s^{-1}$)
V_1	trapping rate of valence band free holes by terminal oxygen ions ($cm^{-3}\,s^{-1}$)
V_{-1}	detrapping rate of valence band free holes by terminal oxygen ions ($cm^{-3}\,s^{-1}$)
V_2	trapping rate of conduction band free electrons by Ti_S^{IV} surface states ($cm^{-3}\,s^{-1}$)
V_{-2}	detrapping rate of trapped electrons at Ti_S^{III} surface states ($cm^{-3}\,s^{-1}$)
V_{r1}	recombination rate of free electrons with surface trapped holes ($cm^{-3}\,s^{-1}$)
V_{r2}	recombination rate of electrons trapped at Ti_S^{III} surface states with surface trapped holes ($cm^{-3}\,s^{-1}$)
V_{r3}	recombination rate of electrons trapped at Ti_S^{III} surface states with valence band free holes ($cm^{-3}\,s^{-1}$)
V_{red}	electroreduction rate of dissolved oxygen species ($cm^{-3}\,s^{-1}$)
QY	quantum yield

Subscripts

st	steady-state conditions
nak	naked electrode
F^-	fluorinated electrode
S	surface
f	free
O$_2$	oxygen saturated electrolyte
N$_2$	nitrogen saturated electrolyte
ox	oxidation

Superscripts

*	illumination conditions
0	dark conditions
i	indirect interfacial transfer of charge
d	direct interfacial transfer of charge

The displacement of single bonded hydroxyl groups by fluoride ions according to reaction (1')

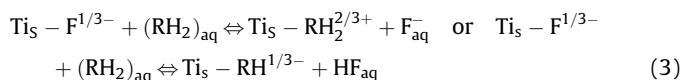$$Ti_S - OH^{1/3-} + F_{aq}^- \Leftrightarrow Ti_S - F^{1/3-} + OH_{aq}^- \tag{1'}$$
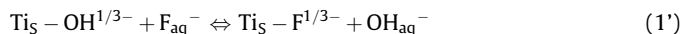
is far less favourable than (1), because: (1) the equilibrium reaction has a pK between 6.5 [6], and 8.0 [1], which means that at the pH = 3.5 employed in experiments reaction (1') is shifted to the left; (2) the adsorption energy of hydroxyl groups exceeds that of water molecules [7]. On the other hand, the displacement of terminal, hydroxyl groups by fluoride ions is highly improbable, as they are twofold coordinated to terminal Ti atoms, while adsorbed water species are only onefold coordinated. Furthermore, according to reaction (1), the TiO$_2$ surface electric charge becomes less positive under surface fluorination, while according to reaction (1') no net change of the surface electric charge takes place.

The competitive adsorption of $(RH_2)_{aq}$ dissolved substrate species and water molecules on the naked TiO$_2$ surface is represented by the exchange reaction:

$$Ti_S - OH_2^{2/3+} + (RH_2)_{aq} \Leftrightarrow Ti_S - RH^{1/3-} + H_3O^+ \tag{2}$$

In contrast, according to the reaction (3), on the fluorinated surface $(RH_2)_{aq}$ adsorption, is hindered to a great extent (shifted to the left), which means modification of TiO$_2$ photocatalytic properties [3,8–15]

$$Ti_S - F^{1/3-} + (RH_2)_{aq} \Leftrightarrow Ti_S - RH_2^{2/3+} + F_{aq}^- \quad \text{or} \quad Ti_s - F^{1/3-}$$
$$+ (RH_2)_{aq} \Leftrightarrow Ti_S - RH^{1/3-} + HF_{aq} \tag{3}$$

According to photocatalytic studies reported in the last few years, TiO$_2$ fluorination seems to increase the photooxidation rate of phenol [3,8–10,14,15] azo dye Acid Red 1 [11,12] benzoic acid [12], tetramethyl ammonium at pH 5–7 [13], and acid orange [14], while decreasing the photooxidation rate of formic acid [12], tetramethyl ammonium at pH 3 [13] and dichloroacetate [14]. The negative effect of fluorination on the photooxidation rate has been attributed mainly to the inhibition of the hole transfer mediated oxidation process, because of the hindered adsorption of the organic substrate on fluorinated TiO$_2$. In contrast, the rate increasing effect has been attributed by some authors not only to decrease of the electron-hole recombination rate, but to the higher availability of photogenerated OH$^\bullet$ radicals in the liquid phase when the TiO$_2$ surface becomes fluorinated [3,8–10,14]. More recently [15], other authors have considered the influence that a negative shift of TiO$_2$ energy levels due to surface fluorination has on the photoinduced charge transfer rate at the semiconductor-electrolyte interface. All these effects will be analyzed here in detail here.

In order to be able to perform a realistic kinetic analysis of the photocatalytic reactions taking place at the semiconductor (TiO$_2$)-aqueous electrolyte interface, we have recently developed a kinetic model, the "Direct–Indirect" (D–I) model [16–20], as an alternative to the nearly universal "Langmuir–Hinshelwood" (L–H) model, which has been applied almost robotically since the 1950s [21].

The L–H model is based on the existence of specific adsorption of RH$_2$ organic substrate species on the semiconductor surface when adsorption is modelled through a Langmuir type isotherm. In contrast, the D–I model, is based on the degree of interaction between (RH$_2$)$_{aq}$ dissolved species with the semiconductor surface, introducing basic concepts, like direct, indirect, adiabatic and inelastic transfer of charge at the semiconductor–electrolyte interface, as fundamental tools [19]. The prevalence of DT on IT, or vice versa, not only depends on the extent of electronic interaction of TiO$_2$-substrate and on the volumetric concentration of substrate dissolved molecules, determining the surface density of chemisorbed species according to an specific adsorption isotherm, but on the illumination intensity. While at low enough values of the illumination flux the IT prevails on the DT mechanism, under high enough photon flux DT prevails on IT [17,19], as shown schematically in Fig. 1. Furthermore, the D–I model predicts a photon flux independent quantum yield for the DT mechanism (case of strong substrate-TiO$_2$ electronic interaction), while for IT, in the absence of specific adsorption of substrate species, an steadily quantum yield decreases as the photon flux increases is predicted, a limiting value of QY = 1 being reached for $\Phi \rightarrow 0$. As will be shown in Section 6, a linear dependence of the QY on $\Phi^{-1/2}$ is also predicted for high enough Φ values.

Here some experimental results and hypothesis found in the literature, concerning the effect of surface fluorination on photocatalytic activity of TiO$_2$, will be critically reviewed in the light of the D–I model.

2. Experimental

All chemicals were used in the experiments as received without further purification. Working solutions were prepared with ultrapure water (Millipore MilliQ, 15 MΩ cm). Sodium perchlorate monohydrate (extra pure) and phenol (extra pure) were supplied by Scharlau. Perchloric acid (p.a., 60%), sodium hydroxide (p.a.), hydrofluoric acid (p.a., 48%) and formic acid (p.a., 99%) were supplied by Merck. The pH of all the solutions was adjusted to 3.5 using 1 M NaOH or 1 M HClO$_4$. Titanium dioxide nanoparticles were supplied by Degussa-Hüls (P25, 20 nm). The oxide slurry for
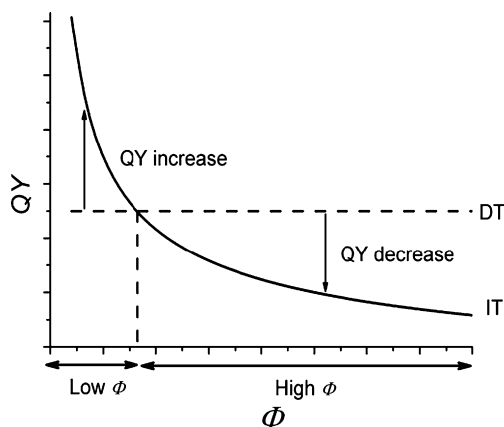

Fig. 1. Schematic representation obtained from Fig. 10 of Ref. [17], of the photooxidation quantum yield (QY) dependence on the photon flux (Φ) predicted by the D–I kinetic model, for both interfacial direct transfer (DT) and indirect transfer (IT) of VB photogenerated holes. Note that for DT a photon flux independent photooxidation quantum yield is predicted, while for IT, in the absence of specific adsorption of substrate species, an steadily quantum yield decreases as the photon flux increases is obtained. For substrates species specifically adsorbed on the TiO$_2$ surface, the photooxidation quantum yield at low enough Φ values is generally determined by adiabatic IT. In contrast, at high enough Φ values (standard experimental conditions), inelastic DT of free holes to reduced species specifically adsorbed on terminal Ti atoms prevails on IT. In the absence of specific adsorption IT is the only working mechanism.

deposition was made using Triton X-100 and acetylaceton 99% from Aldrich.

The nanostructured P25 thin films used in the photoelectrochemical experiments were prepared as follows: 1 g of Degussa P25 powder was ground with a mixture of 30 μL of acetylacetone and 330 μL of distilled water, until the slurry was homogeneous. Next it was diluted with 1.3 mL of distilled water, and 100 μL of the surfactant Triton X-100 were added. 20 μL of the slurry were spread over a (3×1) cm^2 FTO conducting glass plate (U-type TCO glass, Asahi Glass Co., Japan, with a resistance of 10–15 Ω/square) by means of the so-called "Dr Blade" method. It was let to dry in open air for 5 min and finally it was annealed in air for 1 h at 450 °C, giving rise to a 11 μm-thick film as determined by Scanning Electron Microscopy measurements. n-TiO$_2$ films used for impedance measurements were prepared by thermal oxidation in air at 500 °C, for 0.5 h, of 99.9% purity Ti sheet (0.1 cm thick) previously polished to a mirror finish. The depletion layer capacitance (C_{sc}) of the n-TiO$_2$/aqueous electrolyte interface was obtained from measurements of impedance and phase angle [22,23].

The electro- and photoelectrochemical measurements were performed using a standard experimental setup, composed of a computer controlled potentiostat, Wenking-POS 73, and a 150 W Bausch&Lomb Xe arc lamp as illumination source. The electrochemical cell was a conventional three-electrode cell with a 1 mm thick fused silica window, purged with nitrogen (or oxygen). The counter and reference electrodes were a Pt wire and a Ag/AgCl/KCl(sat) electrode, respectively. The working solutions were 0.5 M NaClO$_4$ with 0.01 M (HF + NaF), buffered to pH 3.5. Incident light intensity was measured with an optical power meter (Oriel model 70310) equipped with a thermopile head (Ophir Optronics 71964).

The ATR-FTIR experiments were carried out with a Nicolet Nexus 8700 Spectrometer equipped with a MCT detector. The ATR-FTIR cell was provided with a semi cylindrical ZnSe prism. TiO$_2$ films were deposited on the prism by applying 1.2 μL mm^{-2} of a 0.4 M TiO$_2$ P25 suspension. It was dried in air overnight at 60 °C, yielding a 5 μm-thick film. The spectra were obtained by averaging 50 scans at a resolution of 8 cm^{-1}. ATR-IR spectra of the adsorbate species on TiO$_2$ were recorded with respect to a NaClO$_4$ 0.1 M (pH 3.5) solution as reference. Solution spectra were recorded on the uncoated ZnSe prism.

3. Expected effect of TiO$_2$ fluorination on the quantum yield of photocatalytic oxidation of formic acid and phenol according to the D–I model

Because of the strong specific adsorption in the presence of water, the photooxidation of formic acid (formate ions) on naked TiO$_2$, at low enough pH is a paradigm of interfacial DT of charge [20]. The small frequency shift and the general, drastic intensity increase of the HCOOH-related bands in the presence of the TiO$_2$ film observed in the ATR-IR spectra of Fig. 2a support this thesis. On the other hand, the general signal decrease of formate bands observed when the TiO$_2$ surface becomes fluorinated (Fig. 2b), indicates that the specific adsorption of formate ions is partially inhibited by adsorbed fluoride ions. In contrast, according to the D–I model, an IT photooxidation mechanism has been found to dominate phenol photooxidation [20], which predicts an scarce specific adsorption of this compound on TiO$_2$, as in fact indicates the ATR-IR spectra shown in Fig. 2c, where the presence of a thick nanostructured film of TiO$_2$ does not affect phenol bands intensity. Therefore, phenol photooxidation kinetics should not be affected by TiO$_2$ surface fluorination, in contradiction with the experimental observation that phenol photooxidation rate increases when the naked TiO$_2$ surface becomes fluorinated [3,15]. It has been suggested that this behaviour may be due to a decrease in the
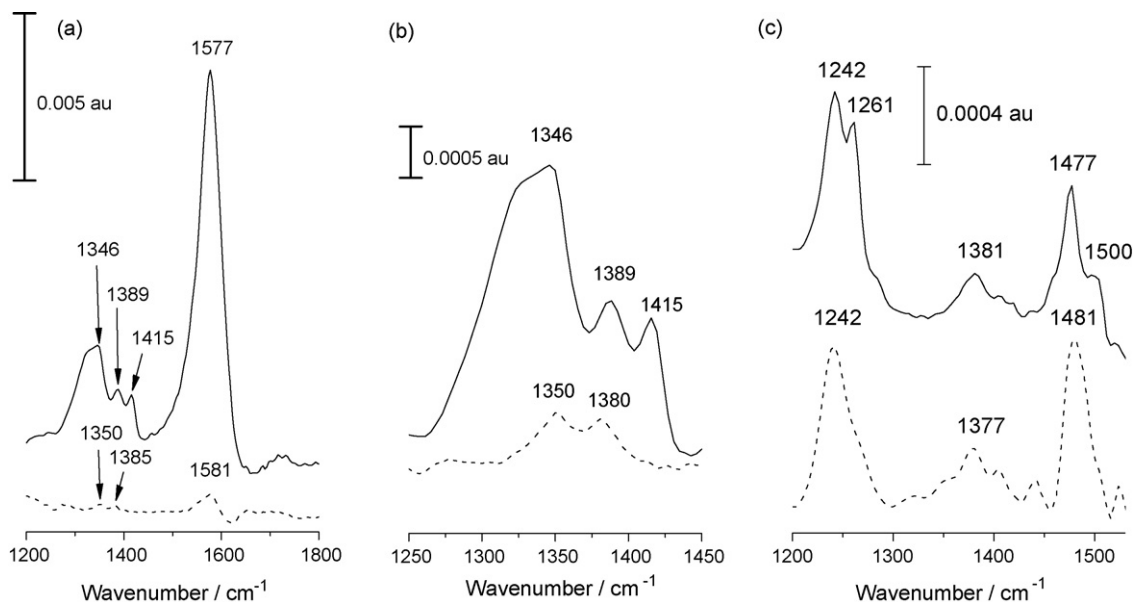
Fig. 2. ATR-IR spectra at room temperature for: (a) 0.01 M formic acid (pH 3.5) in the presence (———) and in the absence (- - - - -) of a 5 μm-thick nanostructured TiO$_2$ (P25) film, the appearing bands being assigned to [35]: 1346 cm^{-1}, symmetric COO group stretching, 1389 cm^{-1}, H–C=O group bending and 1577 cm^{-1} asymmetric COO stretching; (b) 0.01 M formic acid (pH 3.5), without (———) and with 0.01 M (HF + NaF) added (- - - - -). Fluoride was added once the organic was adsorbed at equilibrium. Both spectra were taken in the presence of a 5 nm-thick nanostructured TiO$_2$ (P25) film; (c) 0.01 M phenol (pH 3.5) in the presence (———) and the absence (- - - - -) of a 5 nm-thick nanostructured TiO$_2$ (P25) film. The bands for the solution spectrum can be assigned as follows [36]: 1242 cm^{-1}, C–O stretching, 1381 cm^{-1} in plane C–O–H bending and 1477 and 1500 cm^{-1}, aromatic ring C–C stretching. In all cases the supporting electrolyte was 0.1 M NaClO$_4$.

recombination rate of surface trapped holes with electrons trapped at $Ti_S^{III}-F_S^{4/3-}$ surface states because of the strong electronegativity of fluorine [14,15]. Obviously, a surface recombination rate decrease should induce an increase of the transfer rate of surface trapped holes to $(RH_2)_{aq}$ species. As we will show in Section 5, transient open-circuit photopotential measurements at the TiO$_2$-aqueous electrolyte interface allow to obtain direct information about the influence of surface fluorination on the kinetics of the surface electron-hole recombination process.

4. Influence of surface fluorination on the TiO$_2$ flatband potential

An important parameter defining the concentration of CB electrons and, therefore, affecting electron-hole recombination kinetics, is the semiconductor flatband potential, V_{fb} [22]. It is well known that a change of the semiconductor net surface charge produces a potential drop at the Helmholtz double layer and therefore a V_{fb} shift [22]. According to reaction (1), this should be the behaviour expected under fluorination of the TiO$_2$ surface at pH 3.5, as a decrease of the positive surface electric charge excess is produced, so that a flatband potential shift towards more negative potentials $(-\Delta V_{fb})$ should take place. This hypothesis can be verified form measurements of the depletion layer capacitance (C_{sc}) at the TiO$_2$-electrolyte interface both in the absence and presence of dissolved fluoride ions. In fact, Fig. 3 shows the Mott–Schottky plots obtained for a n-TiO$_2$ polycrystalline thin film in contact with 0.5 M NaClO$_4$ (pH 3.5) without and with addition of 0.01 M (HF + NaF). Since the intercept of the linear plot to the potential axis can be considered as a reliable V_{fb} measurement [22], it is inferred from Fig. 3 that a flatband potential shift between 50 and 60 mV towards negative values is produced under surface fluorination conditions. Similar measurements have been performed recently by Cheng et al. [15], with a TiO$_2$ film prepared by direct thermal oxidation of a Ti sheet in air at 600 °C, and further fluorination by electrode etching in 0.5 M H$_2$SO$_4$ solution containing 0.5% NaF, under anodic polarization. These authors obtained a $V_{fb} \approx -0.21$ V (SCE) for the unetched TiO$_2$, which is shifted

negatively by about 80 mV under fluorination. While these V_{fb} values are slightly more positive than those obtained here, the V_{fb} shift obtained under fluorination is very similar to that obtained by us, as should correspond to a substitution of F$^-$ ions for adsorbed hydroxyl groups.

Since the Helmholtz layer at the TiO$_2$-electrolyte interface behave like a capacitor with a capacitance C_H between 10^{-5} [22] and 4×10^{-5} F cm^{-2} [23], it must be $\Delta V_{fb} = \Delta q/C_H$, where according to (1) Δq represents the increase of surface negative charge due to substitution of specifically adsorbed neutral water molecules by negatively charged fluoride ions ($\Delta q = e[F_s^-]$, $e = 1.6 \times 10^{-19}$ Coul being the elemental electronic charge). Consequently, the following mean value of surface concentration of adsorbed fluoride ions is obtained,

$$[F_s^-] = \frac{\Delta V_{fb} C_H}{e} \approx \frac{0.055 \, V \times 2.5 \times 10^{-5} \, F \, cm^{-2}}{e}$$
$$\approx \frac{1.375 \times 10^{-6} \, Coul \, cm^{-2}}{e} \approx 10^{13} \, ions \, cm^{-2}.$$
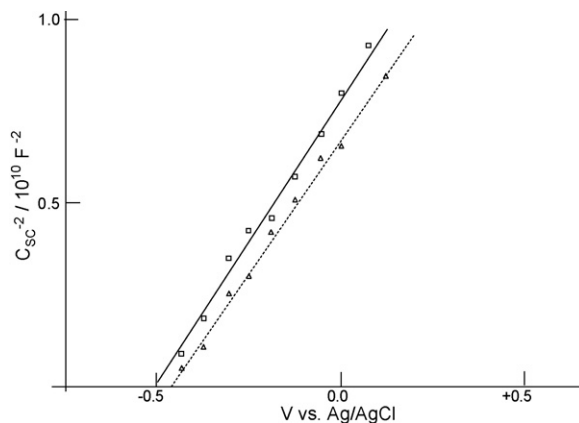

Fig. 3. Mott–Schottky plots of a TiO$_2$ thin film in contact with a 0.5 M NaClO$_4$ aqueous electrolyte (pH 3.5), without (- - - -) and with addition (———) of 0.01 M (HF + NaF). The frequency used was 1 kHz.

This value is in reasonable good agreement with that obtained by Rob van Veen et al. for the surface concentration of fluoride adsorbed on TiO_2 in contact with 0.01 M NaF [24].

5. Influence of surface fluorination on the open-circuit photopotential transients at the TiO_2-aqueous electrolyte interface

5.1. Deoxygenated electrolyte

As pointed out previously [25], the photoelectrochemical behaviour of an illuminated TiO_2 nanostructured electrode in a photoelectrochemical cell under open-circuit conditions is analogous to that of TiO_2 nanoparticles suspended in an electrolyte. In both cases photogenerated electron-hole pairs can either recombine at the semiconductor surface in the absence of suitable electron and hole scavengers in the electrolyte, or be transferred to suitable dissolved electron and/or hole acceptors. The situation of the illuminated nanostructured TiO_2 electrode in contact with a deareated, indifferent aqueous electrolyte (absence of dissolved electron and hole scavengers) under open-circuit conditions is schematized in Fig. 4a. Both photogenerated free holes (h_f^+) and electrons (e_f^-) accumulate at the valence band (VB) and conduction band (CB), respectively at a rate V_0. In a first approximation, it can be assumed that under steady-state illumination conditions the concentrations of CB electrons, $[e_f^-]^*$, VB holes, $[h_f^+]^*$, and Ti_S^{III} species, $[Ti_S^{III}]^*$ satisfy Eqs. (4)–(6)

$$\frac{d[e_f^-]^*}{dt} = V_0 - V_{r1} - V_2 + V_{-2} = 0, \tag{4}$$

$$\frac{d[h_f^+]^*}{dt} = V_0 - V_1 + V_{-1} - V_{r3} = 0 \tag{5}$$

$$\frac{d[Ti_S^{III}]^*}{dt} = V_2 - V_{r2} - V_{r3} - V_{-2} = 0, \tag{6}$$

where V_0 represents the photogeneration rate of $e_f^- - h_f^+$ pairs, V_1 and V_{-1} are the trapping and detrapping rate of VB free holes by surface traps, respectively, ($V_{-1} \ll V_1$ for h_S^+ surface states with an energy kT above E_v), V_2 the trapping rate of free electrons by Ti_S^{IV} intrinsic surface states, V_{-2} the detrapping rate of trapped electrons at Ti_S^{III} surface states ($V_{-2} \ll V_2$ for Ti_S^{III} surface states with an energy about kT below E_c), V_{r1} the $e_f^- - h_S^+$ recombination rate, and V_{r2} and V_{r3} the recombination rate of electrons trapped at

Ti_S^{III} surface states with h_S^+ and h_f^+, respectively. The steady-state open-circuit potential under illumination, (E_{st}^*), is determined by the concentration of conduction band electrons in the dark, $[e_f^-]_{st}^0$ and under illumination, $[e_f^-]_{st}^*$, according to the expression:

$$E_{st}^* = \frac{kT}{q} \ln \frac{[e_f^-]_{st}^*}{[e_f^-]_{st}^0} \tag{7}$$

When illumination is stopped ($V_0 = 0$), the electron-hole recombination process continues in the dark at a rate $V_r = V_{r1} + V_{r2} + V_{r3}$, until a new steady value for the electron concentration in the dark is reached; then an open-circuit voltage E_{st}^0 is measured in the dark. During the relaxation process in the dark, both the CB free electron concentration and the Ti_S^{III} surface states concentration varies with time according to:

$$\frac{d[e_f^-]^0}{dt} = -V_{r1} - V_2 + V_{-2} \tag{8}$$

and

$$\frac{d[Ti_S^{III}]^o}{dt} = V_2 - V_{r2} - V_{r3} - V_{-2}, \tag{9}$$

so that

$$\frac{d[e_f^-]^0}{dt} + \frac{d[Ti_S^{III}]^0}{dt} = -(V_{r1} + V_{r2} + V_{r3}).$$

Since in general $d[T_s^{III}]^0 / d[e_f^-]^0 \ll 1$ [26], the electron concentration decay rate in the dark can be approached by:

$$\frac{d[e_f^-]^0}{dt} = -(V_{r1} + V_{r2} + V_{r3}) \tag{10}$$

As generally accepted, Ti_S represent a continuous distribution of bandgap surface states below the CB edge, acting not only as CB electron traps, but as surface centres for both recombination with VB holes and interfacial electron transfer to oxidized electrolyte species [27]. It can be reasonably assumed on the other hand, that because of the strong electronegativity of fluorine, the effectiveness of Ti_S^{IV} sites as electron traps after F^- complexation will be drastically reduced, which implicates that

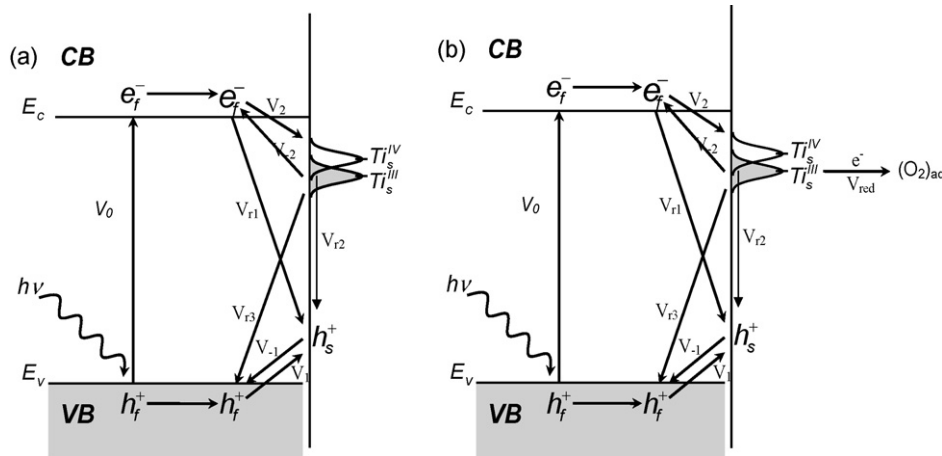$$\left(\frac{d[Ti_S^{III}]^0}{d[e_f^-]^0}\right)_{nak} > \left(\frac{d[Ti_S^{III}]^0}{d[e_f^-]^0}\right)_{F^-}$$

Fig. 4. Schematic energy diagram of the illuminated nanostructured TiO_2 electrode under open-circuit conditions, in contact with: (a) deareated aqueous electrolyte; (b) oxygen saturated electrolyte. V_0 indicates the photogeneration rate of electro-hole pairs, V_1 and V_{-1} the trapping and detrapping rate of free holes by intrinsic surface states, V_2 the trapping rate of free electrons by Ti_S^{IV} intrinsic surface states, V_{-2} the detrapping rate of trapped electrons at Ti_S^{III} surface states, $V_{r,1}$ the recombination rate of conduction band electrons with surface trapped holes, $V_{r,2}$ and $V_{r,3}$ the recombination rate of electrons trapped at Ti_S^{III} surface states with surface trapped holes and free holes, respectively and V_{red} the rate of dissolved oxygen electroreduction.
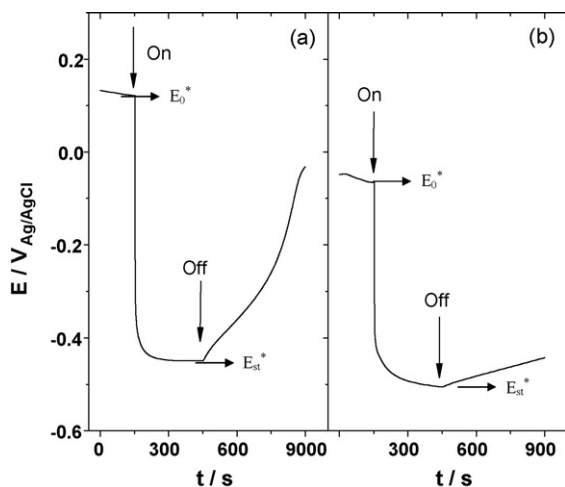
Fig. 5. Time dependence of the open-circuit voltage, at room temperature, in the dark after an illumination period, for a nanostructured TiO$_2$ (P25) electrode either naked (a) or surface fluorinated (b), in contact with a deoxygenated aqueous electrolyte: (a) 0.5 M NaClO$_4$, pH 3.5, (b) 0.5 M NaClO$_4$, 0.01 M (HF + NaF), pH 3.5. Electrode thickness, 10 μm. Electrolyte-electrode side (EE) illumination with a 150 W Xe lamp (incident light power 0.27 W).
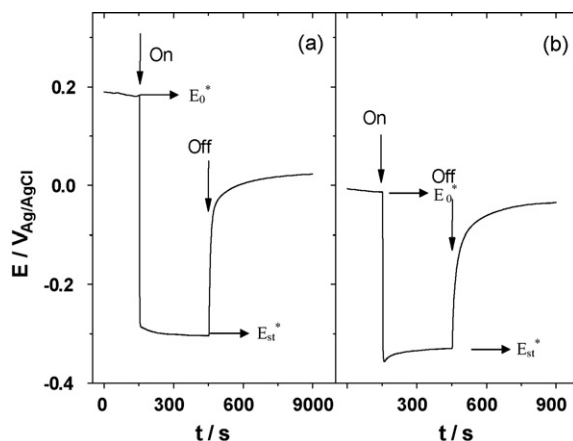

Fig. 6. Time dependence of the open-circuit voltage at room temperature, in the dark after an illumination period, for a nanostructured TiO$_2$ (P25) electrode, either naked (a) or surface fluorinated (b), in contact with an oxygen saturated aqueous electrolyte: (a) 0.5 M NaClO$_4$, pH 3.5, (b) 0.5 M NaClO$_4$, 0.01 M (HF + NaF), pH 3.5. Electrode thickness, 10 μm. Electrolyte-electrode side (EE) illumination with a 150 W Xe lamp (incident light power 0.27 W).

From the time-dependent open-circuit voltage experimental results shown in Fig. 5 for a TiO$_2$ (P25) electrode in contact with an indifferent, deoxygenated aqueous electrolyte, in can be inferred that the initial value of dE^0/dt in the dark, just after an illumination period, decreases from ≈ 0.60 to ≈ 0.15 mV s^{-1} (i.e., about a factor of 4) under electrode fluorination. This indicates that the initial electron concentration decay rate, $d[e_f^-]^0/dt$, and according to (10) the recombination rate of electrons trapped at Ti$_S^{III}$ surface states with surface trapped holes ($V_{r2} = k_{r2}[Ti_s^{III}][h_s^+]$) and/or valence band free holes ($V_{r3} = k_{r3}[Ti_s^{III}][h_f^+]$), slows down when the TiO$_2$ surface becomes fluorinated, an effect mainly due to a decrease of the concentration of Ti surface active centres, $[Ti_S^{III}]$. In fact, a decrease of about one order of magnitude has been estimated recently for the pseudo-first-order surface recombination rate constant of TiO$_2$ (P25) under surface fluorination [28].

5.2. Oxygenated electrolyte

As schematized in Fig. 4b, in the presence of dissolved oxygen, CB electrons are transferred to the electrolyte via an O$_2$ electroreduction process taking place in a two-step interfacial electron transfer mechanism [29]. In the first step (limiting step) CB electrons are transferred inelastically to bandgap surface states associated with Ti$_S^{IV}$ ions, at a rate $V_2 = k_2[Ti_S^{IV}][e_f^-]$, while in a second step electrons trapped at Ti$_S^{III}$ ions are transferred adiabatically to dissolved O$_2$ molecules at a rate $V_{red} = k_{red}[Ti_S^{III}][O_2]_{aq}$, in such a way that

$$V_{red} = V_2 - V_{-2} - V_{r3} - V_{r2} \approx V_2 - V_{r3} - V_{r2}$$
$$= k_2[Ti_s^{IV}][e_f^-] - k_{r2}[Ti_S^{III}][h_S^+] - k_{r3}[Ti_S^{III}][h_f^+]$$

If we compare the time-dependent open-circuit voltage results of Fig. 6 in the oxygenated electrolyte, with those of Fig. 5 for the deoxygenated electrolyte, the following features can be appreciated: (1) During the relaxation process in the dark, dE^0/dt, increases by about a factor of 30 when the electrolyte becomes oxygenated, for the naked electrode, and by about a factor of 100 for the fluorinated electrode. (2) Under electrode fluorination the initial value of dE^0/dt during the relaxation process in the dark diminishes by about a factor of 4 in the N$_2$ saturated electrolyte, while this diminution only reaches about a factor of 1.5 in the O$_2$ saturated electrolyte. (3) In both the N$_2$ and O$_2$ saturated

electrolyte E_{st}^* shifts by 50–60 mV towards negative potentials under surface fluorination, which is equivalent to an increment in the concentration of CB electrons of about one order of magnitude. (4) In both the naked and fluorinated TiO$_2$ E_{st}^* shifts towards positive potentials by about 0.14 V when the electrolyte becomes oxygenated, which means a diminution in the concentration of CB electrons of more than two orders of magnitude

$$\left(\frac{([e_f^-]_{st}^*)_{N_2}}{([e_f^-]_{st}^*)_{O_2}} \approx 10^2 \right).$$

In order to correctly interpret these experimental results, it must be taken into account, according to the scheme of Fig. 4b, that the recombination rate in the oxygen saturated electrolyte is $(V_r)_{O_2} = V_{red} + (V_{r1} + V_{r2} + V_{r3})_{O_2}$, while in the nitrogen saturated electrolyte $(V_r)_{N_2} = (V_{r1} + V_{r2} + V_{r3})_{N_2}$. And taking into account that

$$\frac{(dE^0/dt)_{O_2}}{(dE^0/dt)_{N_2}} = \frac{(V_r)_{O_2}}{(V_r)_{N_2}} = \frac{(V_{r1} + V_{r2} + V_{r3})_{O_2} + V_{red}}{(V_{r1} + V_{r2} + V_{r3})_{N_2}}$$

the increase of dE^0/dt during the relaxation process in the dark when the electrolyte becomes oxygenated, at both the naked and fluorinate electrode, should be attributed to an increase of the density Ti$_S$ centres active in interfacial transfer of conduction band electrons to dissolved O$_2$ molecules and interfacial recombination, in such a way that $(V_{r1} + V_{r2} + V_{r3})_{O_2} + V_{red} > (V_{r1} + V_{r2} + V_{r3})_{N_2}$. On the other hand, the diminution of Ti$_s$ centres under surface fluorination, produces a decrease of the term $(V_{r1} + V_{r2} + V_{r3}) + V_{red}$ in both the oxygen saturated and nitrogen saturated electrolyte, so that dE^0/dt diminishes in both cases. Finally, the observed photovoltage shift between 50 and 60 mV towards negative potentials under surface fluorination ($60\,mV \geq |E_{nak}^* - E_{F^-}^*| = |\Delta E^*| \geq 50\,mV$), in both the deoxygenated and the oxygenated electrolyte, must be attributed to a shift of identical magnitude experimented by the flatband potential of TiO$_2$, as was shown in Section 4.

6. Kinetic analysis of the influence of TiO$_2$ surface fluorination on the photooxidation of specifically adsorbed and non-adsorbed substrates

In order to study the influence of TiO$_2$ surface fluorination on the photooxidation rate of adsorbing and non-adsorbing substrates, we have chosen formic acid and phenol as model organic
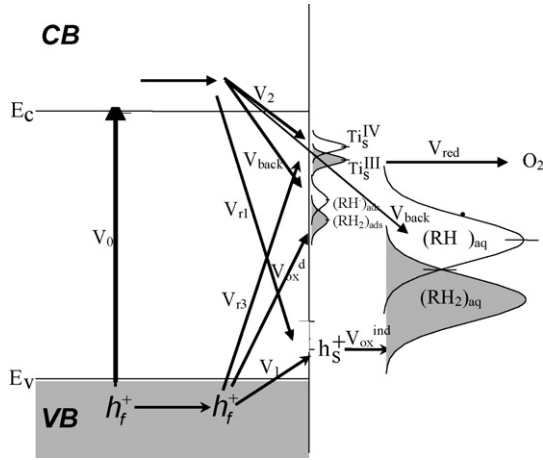
Fig. 7. Energy diagram showing primary reactions of electron-hole generation and recombination, as well as electron and hole transfer to non-adsorbed and specifically adsorbed dissolved species, taking place at the TiO$_2$ electrolyte interface under UV illumination according to the D–I model.

compounds where photooxidation takes place via mechanisms of interfacial DT and IT, respectively [20]. The scheme of Fig. 7 indicates primary recombination and interfacial charge transfer reactions to be considered in the kinetic analysis of photooxidation of specifically adsorbed and non-adsorbed substrate species. The IT photooxidation rate of non-adsorbed species can be written as

$$V_{ox}^i = k_{ox}^i [h_s^+][(RH_2)_{aq}],\qquad(11)$$

while the DT photooxidation rate of specifically adsorbed species is

$$V_{ox}^d = k_{ox}^d [h_f^+][(RH_2)_s],\qquad(12)$$

so that, in general, the quantum yield can be written as:

$$QY = \frac{V_{ox}^d + V_{ox}^i - V_{back}}{V_0}.\qquad(13)$$

However, when both V_{ox}^d and V_{ox}^i represent initial photooxidation rates (i.e., $\lim_{t\to 0}\frac{d[RH_2]}{dt}$), as usually considered in photocatalytic experiments, the term V_{back} is negligible with respect to V_{ox}^d and V_{ox}^i, since for $t \to 0$ [RH$^\bullet$] $\ll$ [(RH$_2$)], so that Eq. (13) becomes:

$$QY \approx QY_{ox}^d + QY_{ox}^i\qquad(13')$$

With the help of the energy diagram in Fig. 7, the following complex mathematical expression for QY_{ox}^i is obtained (see Eq. (A12) of the appendix)

In agreement with a previous analysis of the photooxidation quantum yield for IT, which excluded the participation of bandgap surface states associated to Ti ions in interfacial reactions (see for instance Eq. (18) of Ref. [17]), Eq. (14) indicates that the photooxidation quantum yield of non-adsorbed substrate species depends on the inverse square root of the incident photon flux. Furthermore, Eq. (14) allows to analyze the influence of TiO$_2$ surface fluorination on the quantum yield (QY_{ox}^i). In fact, as it was shown in Section 5, surface fluorination produces a diminution of the concentration of Ti$_S$, surface adsorption centres (both [Ti$_S^{III}$] and [Ti$_S^{IV}$]), so that according to (14) a decrease of QY_{ox}^i should be expected as the TiO$_2$ surface becomes fluorinated.

On the other hand, the following expression is obtained for QY_{ox}^d (see Eq. (A14) of the appendix)

$$QY_{ox}^d = \frac{v_{ox}^d}{v_0}$$
$$= \frac{k_{ox}^d AB[(RH_2)_{aq}]}{(1 + A[(RH_2)_{aq}])(k_1[O_s^{2-}] + k_{r3}[Ti_s^{III}]) + k_{ox}^d AB[(RH_2)_{aq}]}\qquad(15)$$

In contrast with Eq. (14), Eq. (15) indicates a photon flux independent quantum yield for the DT mechanism.

6.1. Influence of TiO$_2$ fluorination on the formic acid (FA) photooxidation quantum yield

Since dissolved FA species, mainly present as formate anions at pH 3.5, strongly interact with the TiO$_2$ surface, both DT and IT mechanisms should participate in their photooxidation mechanism (i.e., QY(FA) = $QY_{ox}^i + QY_{ox}^d$), so that both Eqs. (14) and (15) must be taken into account. However, according to the experimental results by Dijkistra et al., for FA photooxidation on TiO$_2$ (Degussa P-25), in the photon flux range $\rho \le 10^{-4}$ Einst m^{-2} s^{-1} [30], a photon flux independent quantum yield is observed. The same conclusion has been obtained recently by us [20] from FA photooxidation kinetic experimental data by Davidov and Smirnotis [31], indicating that $Q_{ox}^i \ll Q_{ox}^d$, so that for [(RH$_2$)]$_{aq}$ $\equiv$ [FA]$_{aq}$, it can be written:

$$QY_{ox}(FA) \approx QY_{ox}^d(FA)$$
$$= \frac{k_{ox}^d AB[(FA)_{aq}]}{(1 + A[(FA)_{aq}])(k_1[O_s^{2-}] + k_{r3}[Ti_s^{III}]) + k_{ox}^d AB[(FA)_{aq}]}\qquad(16)$$

On the other hand, it has been reported that the rate of FA photooxidation decreases by about a 16% when TiO$_2$ becomes fluorinated [11], (i.e., $(QY)_{ox}^{nack}/(QY)_{ox}^{F^-} \approx 1.2$). This result is congruent with Eq. (16), not only due to the decrease of terms B and [Ti$_S^{III}$], but also of the k_{ox}^d rate constant, which depends on the electronic interaction between the TiO$_2$ surface and dissolved FA

$$QY_{ox}^i = \frac{-k_{ox}^i[(RH_2)_{aq}]k_2[Ti_S^{IV}]}{2k_{r1}k_0\phi} - \frac{k_{r3}[Ti_S^{III}]}{2[k_1[O_S^{2-}] + k_{r3}[Ti_S^{III}] + k_{ox}^d[(RH_2)_S]]} -$$
$$\frac{k_{ox}^d[(RH_2)_S]}{2[k_1[O_S^{2-}] + k_{r3}[Ti_S^{III}] + k_{ox}^d[(RH_2)_S]]} +$$
$$\left\{ \left(\frac{\{k_2[Ti_S^{IV}]k_{ox}^i[(RH_2)_{aq}][k_1[O_S^{2-}] + k_{r3}[Ti_S^{III}] + k_{ox}^d[(RH_2)_S]] + k_0\phi k_{r1}k_{r3}[Ti_S^{III}] + k_0\phi k_{r1}k_{ox}^d[(RH_2)_S]\}}{2k_{r1}k_0\phi[k_1[O_S^{2-}] + k_{r3}[Ti_S^{III}] + k_{ox}^d[(RH_2)_S]]} \right)^2 + \frac{k_{ox}^i k_1[O_S^{2-}][Ti_S^{IV}][(RH_2)_{aq}]}{k_{r1}k_0\phi[k_1[O_S^{2-}] + k_{r3}[Ti_S^{III}] + k_{ox}^d[(RH_2)_S]]} \right\}^{\frac{1}{2}}\qquad(14)$$

species; indeed, a diminution of residual positive charge of the semiconductor surface under fluorination should produce a weaker electrostatic attraction towards negatively charged formate ions.

6.2. Influence of TiO$_2$ fluorination on phenol (PhO) photooxidation quantum yield

In the absence of specific adsorption, as was shown to be the case for phenol in Section 3, photooxidation takes place exclusively via an IT mechanism [17,19,20], so that Eq. (16) must be employed to define the phenol photooxidation quantum yield, which becomes:

$$QY_{ox}^i(PhO) = \frac{-k_{ox}^i[(PhO)_{aq}]k_2[Ti_S^{IV}]}{2k_{r1}k_0\phi} - \frac{k_{r3}[Ti_S^{III}]}{2[k_1[O_S^{2-}]+k_{r3}[Ti_S^{III}]+k_{ox}^d[(PhO)_S]]} -$$
$$\frac{k_{ox}^d[(PhO)_S]}{2[k_1[O_S^{2-}]+k_{r3}[Ti_S^{III}]+k_{ox}^d[(PhO)_S]]} +$$
$$\left\{ \left(\frac{\{k_2[Ti_S^{IV}]k_{ox}^i[(PhO)_{aq}][k_1[O_S^{2-}]+k_{r3}[Ti_S^{III}]+k_{ox}^d[(PhO)_S]]+k_0\phi k_{r1}k_{r3}[Ti_S^{III}]+k_0\phi k_{r1}k_{ox}^d[(PhO)_S]\}}{2k_{r1}k_0\phi[k_1[O_S^{2-}]+k_{r3}[Ti_S^{III}]+k_{ox}^d[(PhO)_S]]}\right)^2 \right.$$
$$\left. +\frac{k_{ox}^i k_1 k_2[O_S^{2-}][Ti_S^{IV}][(PhO)_{aq}]}{k_{r1}k_0\phi\left[k_1[O_S^{2-}]+k_{r3}[Ti_S^{III}]+k_{ox}^d[(PhO)_S]\right]} \right\}^{\frac{1}{2}}$$

(17)

Eq. (17) can be simplified by assuming reasonably that $k_1[O_S^{2-}] \gg k_{r3}[Ti_S^{III}]+k_{ox}^d[(PhO)_S]$, $V_1 \gg V_{r3}$ and $[O_S^{2-}] \gg [Ti_S^{III}]$ [17], resulting:

$$QY_{ox}^i(PhO) \approx -\frac{k_{ox}^i[(PhO)_{aq}]k_2[Ti_S^{IV}]}{2k_{r1}k_0\phi}$$
$$+\left\{ \left(\frac{\{k_2[Ti_S^{IV}]k_{ox}^i[(PhO)_{aq}]\}}{2k_{r1}k_0\phi}\right)^2 + \frac{k_{ox}^i k_2[Ti_S^{IV}][(PhO)_{aq}]}{k_{r1}k_0\phi} \right\}^{\frac{1}{2}}$$

(18)

According to Eq. (18), it can be seen that QY → 1 for Φ → 0. Finally, for high enough photon flux Eq. (18) becomes:

$$QY_{ox}^i(PhO) \approx \left\{ \frac{k_{ox}^i k_2[Ti_S^{IV}][(PhO)_{aq}]}{k_{r1}k_0} \right\}^{\frac{1}{2}} \phi^{-\frac{1}{2}},$$

(19)

which indicates a linear phenol quantum yield dependence on the square root of the photon flux. The same photon flux dependence was obtained in the absence of Ti$_S$ recombination and interfacial electron transfer centres (see for instance Eq. (19) of Ref. [17]),

On the other hand, it has been reported that the rate of phenol photooxidation increases up to about a factor of 3 when TiO$_2$ becomes surface fluorinated [8]. This behaviour that has been explained to be due to the increase of photogenerated OH radical species active in phenol photooxidation as the TiO$_2$ surface becomes fluorinated. Although the photooxidation of surface-bond water species becomes hindered because of the substitution of Ti$_S^{IV}$ bonded water species by F$^-$ ions, the photooxidation of dissolved water species with free VB holes, leading to the generation of free OH$_{aq}^\bullet$ radicals, is strengthened, which results in a higher photooxidant potential [3,8,10–14]. However, this explanation is refutable on the basis of the following arguments: (1) The photooxidation of either adsorbed (Ti$_S^{IV}$ bonded) water species or free (solvated) hydroxyl ions appears to be thermodynamically and kinetically hindered [32]. (2) The same argument should apply in general to the photooxidation of any dissolved compound,

independently on whether they are specifically adsorbed or not, which is not the case, for instance, for formic acid, as its photooxidation quantum yield does not increase but decreases under surface fluorination. (3) It was shown in Section 4 that the equilibrium surface concentration of specifically adsorbed fluoride ions on TiO$_2$ in contact with a 0.01 M NaF + HF aqueous solution at pH 3.5 and room temperature ($[F_S^-] \approx 10^{13}\,cm^{-2}$), is more than one order of magnitude lower than that of a monolayer of adsorbed water ($[H_2O]_{sv} \approx 5 \times 10^{14}\,cm^{-2}$), which indicates that $[H_2O]_S^{F^-} = [H_2O]_s^{nak} - [F_S^-] \approx [H_2O]_s^{nak}$) and, therefore, that the photogeneration rate of adsorbed OH$_S$ radicals should not be appreciably affected by surface fluorination.

According to Eq. (19), a diminution of $[Ti_S^{IV}]$ due to surface fluorination should lead to a phenol photooxidation quantum yield decrease, which is in contradiction with the increase by about a factor of 3 observed experimentally. On the other hand the rate constants k_0 and k_{r1} should not be affected by surface fluorination, but k_2 may decrease because of the repulsive effect of F$^-$ ions adsorbed on terminal Ti atoms on conduction band electrons. However a decrease of k_2 does not implicate an increase, as observed experimentally, but a diminution of $QY_{ox}^i(PhO)$. A simple and reasonable explanation to this experimental observation can be found in the increase of the IT rate constant k_{ox}^i as the TiO$_2$ surface becomes fluorinated. Let us demonstrate that this hypothesis is coherent with the flatband potential shift of about 0.06 V towards negative values observed experimentally in Section 4, as recently claimed by Cheng et al. [15]. In fact, according to the Marcus–Gerischer fluctuating energy model for interfacial transfer
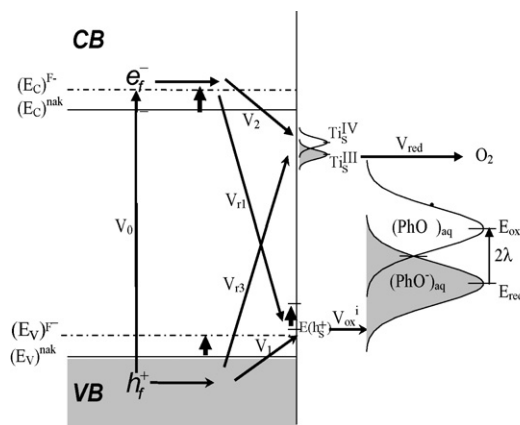

Fig. 8. Energy diagram showing adiabatic, IT of surface trapped holes to non-specifically adsorbed, dissolved phenol species, as well as adiabatic transfer of CB electrons to dissolved oxygen molecules. Note that under surface fluorination TiO$_2$ energy levels are shifted upward between 0.05 and 0.06 eV, while empty end filled phenol energy levels remain pined, so that according Eqs. (19) and (20) the adiabatic hole transfer rate constant k_{ox}^i increases as shown in Table 1.

Table 1
Estimated effect of TiO$_2$ surface fluorination on the IT rate constant, k_{ox}^i, for phenol photooxidation, according to the D–I model, for different values of $E(h_s^+) - E_V$, λ and ΔV_{fb}.

λ(eV)	$[E(h_s^+) - E_V]$ (eV)	$[E_{red}(PhO) - E(h_s^+)]^{nak}$ (eV)	$[k_{ox}^i]^{nak}$(cm^3 s^{-1})	$[E_{red}(PhO) - E(h_s^+)]^{F^-}$ (eV)	$[k_{ox}^i]^{F^-}$ (cm^3 s^{-1})	$\left(\frac{[k_{ox}^i]^{F^-}}{[k_{ox}^i]^{nak}}\right)^{1/2}$	ΔV_{fb} (eV)
0.7	0.1	1.2	4.6×10^{-10}	1.15	2.3×10^{-9}	2.2	0.05
0.7	0.2	1.1	1.1×10^{-8}	1.04	6.3×10^{-8}	2.4	0.06
0.6	0.1	1.3	3.1×10^{-13}	1.25	2.4×10^{-12}	2.8	0.05
0.6	0.2	1.2	1.7×10^{-11}	1.14	1.6×10^{-10}	3.1	0.06

k_{ox}^i values were estimated according to the Marcus-Gerischer expression: $k_{ox}^i \propto \exp - \left[\frac{(E_{red}(PhO) - E(h_s^+))^2}{4\lambda kT}\right]$.

of charge under weak semiconductor-electrolyte electronic interaction [33], the photooxidation rate constant for IT can be defined by the expression:

$$k_{ox}^i(PhO) = A' \exp - \left[\frac{(E_{red}(PhO) - E(h_s^+))^2}{4\lambda kT}\right], \tag{20}$$

where A' is a constant, $E(h_s^+)$ is the energy of holes trapped at O_S^{2-} surface states located just above the VB edge (E_v) [32], $E_{red}(PhO)$ is the most probable value of the Gaussian distribution of filled energy levels corresponding to dissolved phenol species and λ is the reorganization energy of the $(PhO/PhO^•)$ redox couple. $k_{ox}^i(PhO)$ can be evaluated from (20), with the help of the energy diagram of Fig. 8, on the basis that $E_{redox}^0(PhO) - E_v(TiO_2)^{nak} \approx 2.0\,V$ [34],

$$E_{red}(PhO) - E(h_s^+)^{nak} = \left[E_{redox}^0(PhO) - E_v^{nak} - \lambda\right] - (E(h_s^+) - E_v)^{nak},$$

$$E_{red}(PhO) - E(h_s^+)^{F^-} = \left[E_{redox}^0(PhO) - E_v^{F^-} - \lambda\right]$$
$$- (E(h_s^+) - E_v)^{F^-}, \qquad (E(h_s^+) - E_v)^{nak}$$
$$= (E(h_s^+) - E_v)^{F^-}$$

and

$$E_v^{F^-} - E_v^{nak} = E^{F^-}(h_s^+) - E^{nak}(h_s^+) = \Delta V_{fb} \approx 0.06\,V.$$

Table 1 shows interfacial hole transfer rate constant values for PhO photooxidation at the naked $((k_{ox}^i)^{nak})$ and fluorinated surface $((k_{ox}^i)^{F^-})$, estimated from Eq. (20) for reasonable values of the reorganization energy between 0.7 and 0.6 eV [22], and of $E(h_s^+)$ between 0.1 and 0.2 eV above the TiO$_2$ VB edge [32]. According to Eq. (19),

$$\frac{(QY_{ox}^i)^{F^-}}{(QY_{ox}^i)^{nak}} \approx \left(\frac{(k_{ox}^i)^{F^-}}{(k_{ox}^i)^{nak}}\right)^{1/2} \left(\frac{[Ti_s^{IV}]^{F^-}}{[Ti_s^{IV}]^{nak}}\right)^{\frac{1}{2}}$$

and taking into account that

$$[Ti_S]^{F^-} = [Ti_S]^{nak} - [F_s^-] = 5 \times 10^{14} - 10^{13}\,cm^{-2} = 4.9 \times 10^{14}\,cm^{-2},$$

it can be written that

$$\left(\frac{[Ti_s^{IV}]^{F^-}}{[Ti_s^{IV}]^{nak}}\right)^{\frac{1}{2}} \approx \left(\frac{4.9 \times 10^{14}\,cm^{-2}}{5 \times 10^{14}\,cm^{-2}}\right)^{\frac{1}{2}} \approx 0.99$$

so that

$$\frac{(QY_{ox}^i)^{F^-}}{(QY_{ox}^i)^{nak}} \approx \left(\frac{(k_{ox}^i)^{F^-}}{(k_{ox}^i)^{nak}}\right)^{1/2}$$

and, therefore, the value of $((QY_{ox}^i)^{F^-}/(QY_{ox}^i)^{nak}) \approx 3$ found experimentally is in reasonable good agreement with the estimated values reported in Table 1.

7. Conclusions

The analysis of open-circuit potential transients and impedance measurements at the TiO$_2$-electrolyte interface under different experimental conditions indicates that TiO$_2$ surface fluorination in 0.01 M HF + NaF aqueous solution (pH 3.5), is responsible of the following main effects: (1) a net decrease of positive electric charge at the semiconductor surface due to the substitution of water molecules adsorbed at terminal Ti atoms by fluoride ions, resulting in a concentration of specifically adsorbed F$^-$ species of the order of 10^{13} cm^{-2}; (2) a parallel diminution of the concentration of surface sites associated with terminal Ti atoms, active in the specific adsorption of dissolved substrate species; (3) a diminution of surface recombination centres associated with terminal $[Ti_S^{IV}]$ ions; (4) a simultaneous lessening of the surface electron-hole recombination rate and dissolved oxygen electroreduction rate.

According to the D–I kinetic model, the consequence of these effects on the photooxidation kinetics of substrate species can be resumed as follows: under surface fluorination the specific adsorption of dissolved substrates species on terminal Ti atoms becomes inhibited and a diminution of the photooxidation rate is produced when the DT mechanism prevails on the IT mechanism, as experimentally observed for formic acid [20]. In contrast, when the electronic interaction of substrate species with the TiO$_2$ surface is weak, as it is the case for phenol [20], the induced upward flatband potential shift produces an increased overlapping between empty electronic energy levels of surface trapped holes and filled energy levels of reduced, dissolved substrate species, which leads to an increase of the IT photooxidation rate constant.

The photocatalytic mechanism of phenol degradation, invoking the increasing participation of free OH$_{aq}^•$ radicals generated by direct photooxidation of free water species with BV holes should be ruled out as neither free nor surface-bound water species can be photooxidized with VB holes. The only radical species active in oxidative photocatalytic processes should be: (a) VB free holes able to react inelastically with specifically adsorbed substrates; (b) holes trapped at terminal twofold coordinated bridging oxygen ions able to be transferred adiabatically to reduced, dissolved substrates; (c) free OH$^•$ radicals, superoxide radicals and/or H$_2$O$_2$ species generated via interfacial transfer of photogenerated conduction band electrons to dissolved O$_2$.

Appendix A

Under pseudo-steady-state conditions the following equalities can be written with the help of the energy diagram in Fig. 7 [17]:

$$V_0 = k_0 \varphi \tag{A1}$$

where k_0 is a constant parameter and φ is the incident photon flux,

$$\frac{d[e_f^-]}{dt} \approx V_0 - V_{r1} - V_2 = 0, \tag{A2}$$

$$\frac{d[h_f^+]}{dt} \approx V_0 - V_1 - V_{r3} - V_{ox}^d = 0, \tag{A3}$$

$$V_1 = V_{r1} + V_{ox}^i, \tag{A4}$$

so that combining (A3) and (A4) we have

$$V_{r1} = V_0 - V_{ox}^i - V_{r3} - V_{ox}^d \tag{A5}$$

Developing (A2) we obtain that

$$[e_f^-] = \frac{k_0 \phi}{k_{r1}[h_s^+] + k_2[Ti_s^{IV}]}, \tag{A6}$$

while developing (A3) and (A5) it is

$$[h_f^+] = \frac{k_0 \phi}{k[O_s^{2-}] + k_{r3}[Ti_s^{III}] + k_{ox}^d[RH_2]_s} \tag{A7}$$

and

$$[e_f^-] = \frac{k_0 \phi - k_{ox}^i[h_s^+][(RH_2)_{aq}] - k_{r3}[h_f^+][Ti_s^{III}] - k_{ox}^d[h_f^+][(RH_2)_s]}{k_{r1}[h_s^+]}, \tag{A8}$$

where the concentration of specifically adsorbed species, $(RH_2)_S$, can be approached by a Langmuir type adsorption isotherm.

$$[(RH_2)_s] = \frac{AB[(RH_2)_{aq}]}{1 + A[(RH_2)_{aq}]}, \tag{A9}$$

A being the adsorption constant of dissolved substrate species on TiO_2 and B the concentration of TiO_2 surface sites where adsorption takes place ($B \approx [Ti_S]$). On the other hand, by combining (A6), (A7) and (A8) expression (A10) is obtained for the concentration of surface trapped holes.

$$
\begin{aligned}
[h_S^+] = {} & \frac{-k_2[Ti_S^{IV}]}{2k_{r1}} - \frac{k_0 \phi k_{r3}[Ti_S^{III}]}{2k_{ox}^i[(RH_2)_{aq}][k_1[O_S^{2-}] + k_{r3}[Ti_S^{III}] + k_{ox}^d[(RH_2)_S]]} - \\
& \frac{k_0 \phi k_{ox}^d[(RH_2)_S]}{2k_{ox}^i[(RH_2)_{aq}][k_1[O_S^{2-}] + k_{r3}[Ti_S^{III}] + k_{ox}^d[(RH_2)_S]]} + \\
& \left\{ \left(\frac{k_2[Ti_S^{IV}]k_{ox}^i[(RH_2)_{aq}][k_1[O_S^{2-}] + k_{r3}[Ti_S^{III}] + k_{ox}^d[(RH_2)_S]] + k_0 \phi k_{r1} k_{r3}[Ti_S^{III}] + k_0 \phi k_{r1} k_{ox}^d[(RH_2)_S]}{2k_{ox}^i k_{r1}[(RH_2)_{aq}][k_1[O_S^{2-}] + k_{r3}[Ti_S^{III}] + k_{ox}^d[(RH_2)_S]]} \right)^2 \right. \\
& \left. + \frac{k_0 \phi k_1 k_2[O_S^{2-}][Ti_S^{IV}]}{k_{ox}^i k_{r1}[(RH_2)_{aq}][k_1[O_S^{2-}] + k_{r3}[Ti_S^{III}] + k_{ox}^d[(RH_2)_S]]} \right\}^{\frac{1}{2}}
\end{aligned}
\tag{A10}
$$

Further, by considering that

$$QY_{ox}^i = \frac{v_{ox}^i}{v_0} = \frac{k_{ox}^i[RH_2]_{aq}}{k_0 \varphi}[h_S^+], \tag{A11}$$

the following expression is obtained for the quantum yield for IT by combining (A10) and (A11)

$$QY_{ox}^i = \frac{-k_{ox}^i[(RH_2)_{aq}]k_2[Ti_S^{IV}]}{2k_{r1}k_0\phi} - \frac{k_{r3}[Ti_S^{III}]}{2[k_1[O_S^{2-}] + k_{r3}[Ti_S^{III}] + k_{ox}^d[(RH_2)_S]]} -$$

$$\frac{k_{ox}^d[(RH_2)_S]}{2[k_1[O_S^{2-}] + k_{r3}[Ti_S^{III}] + k_{ox}^d[(RH_2)_S]]} +$$

$$\left\{ \left(\frac{\{k_2[Ti_S^{IV}]k_{ox}^i[(RH_2)_{aq}][k_1[O_S^{2-}] + k_{r3}[Ti_S^{III}] + k_{ox}^d[(RH_2)_S]] + k_0\phi k_{r1}k_{r3}[Ti_S^{III}] + k_0\phi k_{r1}k_{ox}^d[(RH_2)_S]\}}{2k_{r1}k_0\phi[k_1[O_S^{2-}] + k_{r3}[Ti_S^{III}] + k_{ox}^d[(RH_2)_S]]} \right)^2 \right. $$
$$\left. + \frac{k_{ox}^i k_1 k_2[O_S^{2-}]\left[Ti_S^{IV}\right][(RH_2)_{aq}]}{k_{r1}k_0\phi[k_1[O_S^{2-}] + k_{r3}[Ti_S^{III}] + k_{ox}^d[(RH_2)_S]]} \right\}^{\frac{1}{2}} \tag{A12}$$

On the other hand, taking into account that

$$V_{ox}^d = k_{ox}^d[h_f^+][(RH_2)_S], \tag{A13}$$

the following expression is obtained for DT quantum yield by combining (A1), (A7), (A8) and (A13):

$$QY_{ox}^d = \frac{v_{ox}^d}{v_0} = \frac{k_{ox}^d AB[(RH_2)_{aq}]}{(1 + A[(RH_2)_{aq}])(k_1[O_S^{2-}] + k_{r3}[Ti_S^{III}]) + k_{ox}^d AB[(RH_2)_{aq}]} \tag{A14}$$

References

[1] M.R. Hoffmann, S.T. Martin, W. Choi, D. Bahnemann, Chem. Rev. 95 (1995) 69.
[2] M. Abdullah, G.K.C. Low, R.W. Mathews, J. Phys. Chem. 94 (1990) 6820.
[3] C. Minero, G. Mariella, V. Maurino, E. Pelizzetti, Langmuir 16 (2000) 2632.
[4] T. Hiemstra, W.H. van Riemsdijk, G.H. Bolt, J. Colloid Interf. Sci. 179 (1989) 91.
[5] T. Hiemstra, W.H. van Riemsdijk, G.H. Bolt, J. Colloid Interf. Sci. 179 (1989) 105.
[6] C.A. Giacomelli, M.J. Avena, C.P. De Pauli, Langmuir 11 (1998) 3483.
[7] Y. Suda, T. Morimoto, Langmuir 3 (1987) 786.
[8] C. Minero, G. Mariella, V. Maurino, D. Vione, E. Pelizzetti, Langmuir 16 (2000) 8964.
[9] P. Calza, E. Pelizzetti, Pure Appl. Chem. 73 (2001) 1839.
[10] J.S. Park, W. Choi, Langmuir 20 (2004) 11523.
[11] M. Mrowetz, E. Selli, Phys. Chem. Chem. Phys. 7 (2005) 1100.
[12] M. Mrowetz, E. Selli, New J. Chem. 30 (2006) 108.
[13] M.S. Vohra, S. Kim, W. Choi, J. Photochem. Photobiol. A: Chem. 160 (2003) 55.
[14] H. Park, W. Choi, J. Phys. Chem. B 108 (2004) 4086.
[15] X.F. Cheng, W.H. Leng, D.P. Liu, Y.M. Xu, J.Q. Zang, C.N. Cao, J. Phys. Chem. C 112 (2008) 8725.
[16] T. Lana-Villarreal, R. Gómez, M. Neumann-Spallart, N. Alonso-Vante, P. Salvador, J. Phys. Chem. B 108 (2004) 15172.
[17] T. Lana-Villarreal, R. Gómez, M. González, P. Salvador, J. Phys. Chem. B 108 (2004) 20278.
[18] I. Mora-Seró, T. Lana-Villarreal, J. Bisquert, A. Pitarch, R. Gómez, P. Salvador, J. Phys. Chem. B 109 (2005) 3371.
[19] D. Monllor-Satoca, R. Gómez, M. González-Hidalgo, P. Salvador, Catal. Today 129 (1/2) (2007) 247.
[20] J.F. Montoya, J. Velásquez, P. Salvador, Appl. Catal. B: Environ. 88 (2009) 50.
[21] A.V. Emeline, V.K. Ryabchuk, N. Serpone, J. Phys. Chem. B 109 (2005) 18515.
[22] S.R. Morrison, Electrochemistry at Semiconductors and Oxidized Metal Electrodes, Plenum Press, New York, 1980.
[23] M. Tomkiewicz, J. Electrochem. Soc. 126 (1979) 1505.
[24] J.A. Rob van Veen, F.T.G. Veltmaat, G. Jonkers, J. Chem. Soc., Chem. Commun. (1985) 1656.
[25] R. Gómez, P. Salvador, Solar Energy Mat. Solar Cells 88 (2005) 377.
[26] J. Bisquert, V.S. Vikhrenko, J. Phys. Chem. B 108 (2004) 2313.
[27] P. Salvador, M. Gonzalez-Hidalgo, A. Zaban, J. Bisquert, J. Phys. Chem. B. 109 (2005) 15915.
[28] D. Monllor-Satoca, R. Gomez, J. Phys. Chem. C 112 (2008) 139.
[29] D. Tafalla, P. Salvador, Ber. Bunsenges. Phys. Chem. 91 (1987) 475.
[30] M.F.J. Dijkstra, H.J. Pannemann, J.G.M. Winkelman, J.J. Kelly, A.A.C.M. Beenackers, Chem. Eng. Sci. 57 (2002) 4895.
[31] L. Davydov, P.G. Smirnotis, J. Catal. 191 (2000) 105.
[32] P. Salvador, J. Phys. Chem. C 111 (2007) 17038.
[33] H. Gerischer, Surf. Sci. 18 (1969) 97.
[34] E. Pelizzetti, C. Minero, Electrochim. Acta 38 (1993) 47.
[35] F.P. Rotzinger, J.M. Kesselman-Truttmann, S.J. Hug, V. Shklover, M. Grätzel, J. Phys. Chem. B 108 (2004) 5004.
[36] H. Günzler, H.-U. Gremlich, IR Spectroscopy. An Introduction, Wiley-VCH, 2002.